Liquid Crystals
Publication details, including instructions for authors and subscription information:
http://www.informaworld.com/smpp/title~content=t713926090

Computer simulation of chiral liquid crystal phases. I. The polymorphism of the chiral Gay-Berne fluid

R. Memmer[a]; H. -G. Kuball[a]; A. Schönhofer[b]
[a] Fachbereich Chemie, Universität Kaiserslautern, Kaiserslautern, Germany [b] Technische Universität Berlin, Berlin, Germany

To cite this Article Memmer, R. , Kuball, H. -G. and Schönhofer, A.(1993) 'Computer simulation of chiral liquid crystal phases. I. The polymorphism of the chiral Gay-Berne fluid', Liquid Crystals, 15: 3, 345 — 360
To link to this Article: DOI: 10.1080/02678299308029136
URL: http://dx.doi.org/10.1080/02678299308029136

LIQUID CRYSTALS, 1993, VOL. 15, NO. 3, 345–360

Computer simulation of chiral liquid crystal phases
I. The polymorphism of the chiral Gay–Berne fluid†

by R. MEMMER* and H.-G. KUBALL
Fachbereich Chemie, Universität Kaiserslautern,
D-67663 Kaiserslautern, Germany

and A. SCHÖNHOFER
Technische Universität Berlin, D-10623 Berlin, Germany

(*Received 5 January 1993; accepted 10 May 1993*)

We report the results of computer simulation studies for a bulk system composed of chiral particles interacting via the Gay–Berne potential and an additive chiral potential. Using Monte Carlo (MC) simulations in the *NVT* ensemble, the chirality–temperature plane of the phase diagram was studied at different points by a variation of the chirality parameter c describing the strength of the chiral potential. Additionally to the well-known isotropic, nematic and smectic phases of the Gay–Berne fluid, we localized regions of cholesteric phase. For large values of the chirality parameter we also observed blue phases. Furthermore, when starting from a cholesteric phase and decreasing the temperature at constant c, we obtained a phase region showing characteristics of the recently discovered helical smectic A* phase. All phases have been characterized by correlation functions, order parameters, and visual representations of selected configurations. All results of the simulation are limited by the small system size of $N = 256$ molecules and the use of periodic boundary conditions.

1. Introduction

The computer simulation of liquid crystals gains more and more importance, favoured especially through the rapid development of computer hardware which enables the simulation of systems with increasing complexity [1]. The first simulations have been restricted to the study of lattice models, for example, the Lebwohl–Lasher model [2]. A lot of recent work was carried out, for example, by Frenkel *et al.* [3–5], in order to investigate fluids composed of non-spherical hard body molecules, i.e. simulations related to Onsager's model [6]. Nowadays, however, the results of simulations using more realistic atom-based models, including total translational and rotational degrees of freedom and intramolecular flexibility, have been reported, as in the case of the molecular dynamics (MD) studies of Wilson and Allen [7, 8].

A model which includes both anisotropic short range repulsive, as well as anisotropic long range attractive interactions, without being restricted by the extremely time consuming complexity of atom-based models is provided by a model potential introduced by Gay and Berne [9] as a modification of the gaussian overlap model generalized to a Lennard–Jones form [10]. This potential has been extensively

* Author for correspondence.

† Presented at the Fourteenth International Liquid Crystal Conference, 21–26 June 1992, University of Pisa, Italy.

0267–8292/93 $10·00

studied during the past years as a model system for liquid crystals, beginning with Luckhurst *et al.* [11–14], and by De Miguel *et al.* [15, 16], investigating their isotropic, nematic and smectic phases.

In spite of these successful simulations of nematic and smectic liquid crystal phases, relatively little work has been published about the simulation of chiral phases (see for instance [17]), although chirality generates, in addition to cholesteric phases a lot of phases with complex structures [18], as in the case of the different blue phases [19] or even the recently discovered helical smectic A* phase [20]. The aim of our study is to investigate the influence of chirality on liquid crystal phases by performing MC simulations on model systems based on the Gay–Berne potential and taking into account a chirality-producing potential term.

2. Chiral model potential

The intermolecular interactions between two chiral molecules i and j separated by an intermolecular vector $\mathbf{r}$ with orientations denoted by Ω_i and Ω_j respectively, are described here by the pair potential

$$U(\Omega_i, \Omega_j, \mathbf{r}) = aU_a(\Omega_i, \Omega_j, \mathbf{r}) + cU_c(\Omega_i, \Omega_j, \mathbf{r}), \tag{1}$$

where a and c measure the strength of the achiral interaction potential U_a and the chiral interaction potential U_c, respectively. The additive form is chosen for reasons of computational simplicity.

The achiral interaction potential U_a is the Gay–Berne potential [9]

$$\begin{aligned} U_a(\Omega_i, \Omega_j, \mathbf{r}) &= U_a(\hat{\mathbf{u}}_i, \hat{\mathbf{u}}_j, \mathbf{r}) \\ &= 4\varepsilon(\hat{\mathbf{u}}_i, \hat{\mathbf{u}}_j, \hat{\mathbf{r}}) \left\{ \left(\frac{\sigma_0}{r - \sigma(\hat{\mathbf{u}}_i, \hat{\mathbf{u}}_j, \hat{\mathbf{r}}) + \sigma_0} \right)^{12} - \left(\frac{\sigma_0}{r - \sigma(\hat{\mathbf{u}}_i, \hat{\mathbf{u}}_j, \hat{\mathbf{r}}) + \sigma_0} \right)^{6} \right\}, \end{aligned} \tag{2}$$

where $\hat{\mathbf{u}}_i$, $\hat{\mathbf{u}}_j$ are unit vectors describing the orientation of two rotationally symmetric particles. $\hat{\mathbf{r}}$ denotes the unit vector parallel to $\mathbf{r}$ and $r = |\mathbf{r}|$ the molecular separation.

The explicit expressions for the orientation-dependent parameters $\sigma(\hat{\mathbf{u}}_i, \hat{\mathbf{u}}_j, \hat{\mathbf{r}})$ and $\varepsilon(\hat{\mathbf{u}}_i, \hat{\mathbf{u}}_j, \hat{\mathbf{r}})$ are given by

$$\sigma(\hat{\mathbf{u}}_i, \hat{\mathbf{u}}_j, \hat{\mathbf{r}}) = \sigma_0 \left[1 - (\chi/2) \left\{ \frac{(\hat{\mathbf{r}}\cdot\hat{\mathbf{u}}_i + \hat{\mathbf{r}}\cdot\hat{\mathbf{u}}_j)^2}{1 + \chi(\hat{\mathbf{u}}_i\cdot\hat{\mathbf{u}}_j)} + \frac{(\hat{\mathbf{r}}\cdot\hat{\mathbf{u}}_i - \hat{\mathbf{r}}\cdot\hat{\mathbf{u}}_j)^2}{1 - \chi(\hat{\mathbf{u}}_i\cdot\hat{\mathbf{u}}_j)} \right\} \right]^{-1/2}, \tag{3}$$

and

$$\varepsilon(\hat{\mathbf{u}}_i, \hat{\mathbf{u}}_j, \hat{\mathbf{r}}) = \varepsilon_0 [\varepsilon(\hat{\mathbf{u}}_i, \hat{\mathbf{u}}_j)]^{\nu} [\varepsilon'(\hat{\mathbf{u}}_i, \hat{\mathbf{u}}_j, \hat{\mathbf{r}})]^{\mu}, \tag{4}$$

with

$$\varepsilon(\hat{\mathbf{u}}_i, \hat{\mathbf{u}}_j) = [1 - \chi^2(\hat{\mathbf{u}}_i\cdot\hat{\mathbf{u}}_j)^2]^{-1/2}, \tag{5}$$

and

$$\varepsilon'(\hat{\mathbf{u}}_i, \hat{\mathbf{u}}_j, \hat{\mathbf{r}}) = 1 - (\chi'/2) \left\{ \frac{(\hat{\mathbf{r}}\cdot\hat{\mathbf{u}}_i + \hat{\mathbf{r}}\cdot\hat{\mathbf{u}}_j)^2}{1 + \chi'(\hat{\mathbf{u}}_i\cdot\hat{\mathbf{u}}_j)} + \frac{(\hat{\mathbf{r}}\cdot\hat{\mathbf{u}}_i - \hat{\mathbf{r}}\cdot\hat{\mathbf{u}}_j)^2}{1 - \chi'(\hat{\mathbf{u}}_i\cdot\hat{\mathbf{u}}_j)} \right\}. \tag{6}$$

The parameters

$$\chi = \{(\sigma_e/\sigma_s)^2 - 1\}/\{(\sigma_e/\sigma_s)^2 + 1\}, \tag{7}$$

and

$$\chi' = \{1 - (\varepsilon_e/\varepsilon_s)^{1/\mu}\}/\{1 + (\varepsilon_e/\varepsilon_s)^{1/\mu}\}, \tag{8}$$

are related to σ_e/σ_s, reflecting the shape anisotropy and to $\varepsilon_e/\varepsilon_s$, reflecting the anisotropy in the well depth comparing the end to end (e) and side by side (s) configuration. These functions have been discussed in detail by Luckhurst *et al.* [12], who introduced a model nematogen and identified its different phases by MD simulations.

The chiral interaction potential U_c must be pseudo-scalar and is additionally chosen to be invariant against the substitution $\hat{\mathbf{u}}_i \rightarrow -\hat{\mathbf{u}}_i$ or $\hat{\mathbf{u}}_j \rightarrow -\hat{\mathbf{u}}_j$ (head–tail symmetry). The simplest expression with these properties which can be formed from the three unit vectors $\hat{\mathbf{u}}_i$, $\hat{\mathbf{u}}_j$, and $\hat{\mathbf{r}}$ is $[(\hat{\mathbf{u}}_i \times \hat{\mathbf{u}}_j)\cdot\hat{\mathbf{r}}]\,(\hat{\mathbf{u}}_i \cdot \hat{\mathbf{u}}_j)$. A separation–dependent factor, chosen for computational convenience to be of the Gay–Berne type, is used with the exponent 7. (A term $r^{-7}\,[(\hat{\mathbf{u}}_i \times \hat{\mathbf{u}}_j)\cdot\hat{\mathbf{r}}]\,(\hat{\mathbf{u}}_i \cdot \hat{\mathbf{u}}_j)$ also results in the multipole expansion of the interaction energy of two chiral molecules [21, 22]. It is worth mentioning that results similar to those discussed in the following sections can be obtained independently of the exponent chosen for the separation-dependent factor as tested by us using the exponent 11.) We arrive thus at the expression

$$U_c(\Omega_i, \Omega_j, \mathbf{r}) = U_c(\hat{\mathbf{u}}_i, \hat{\mathbf{u}}_j, \hat{\mathbf{r}})$$

$$= 4\varepsilon(\hat{\mathbf{u}}_i, \hat{\mathbf{u}}_j, \hat{\mathbf{r}})\left(\frac{\sigma_0}{r - \sigma(\hat{\mathbf{u}}_i, \hat{\mathbf{u}}_j, \hat{\mathbf{r}}) + \sigma_0}\right)^7 [(\hat{\mathbf{u}}_i \times \hat{\mathbf{u}}_j)\cdot\hat{\mathbf{r}}]\,(\hat{\mathbf{u}}_i \cdot \hat{\mathbf{u}}_j). \tag{9}$$

In order to illustrate the influence of the chiral interaction potential we show, in figure 1, the variation of the scaled potential energy $U^* = U/\varepsilon_0$, and separately its chiral and achiral part for a pair of molecules with dependence on the twist angle δ describing the rotation around the intermolecular distance vector $\mathbf{r}$ for a selected configuration. Contrary to the achiral situation at $c = 0$ where, for the parameter values of a rod-like molecule given in § 3, the energetic minimum is at $\delta = 0$ (side by side configuration), at $c \neq 0$ a tilted orientation is now favoured. The influence of the chirality parameter c on the value of the most preferred twist angle is shown in figure 2 in the form of the contours of U^* in a plane with c and δ as orthogonal cartesian coordinates. A change of sign of c simply yields a favoured orientation with $-\delta$ instead of δ.

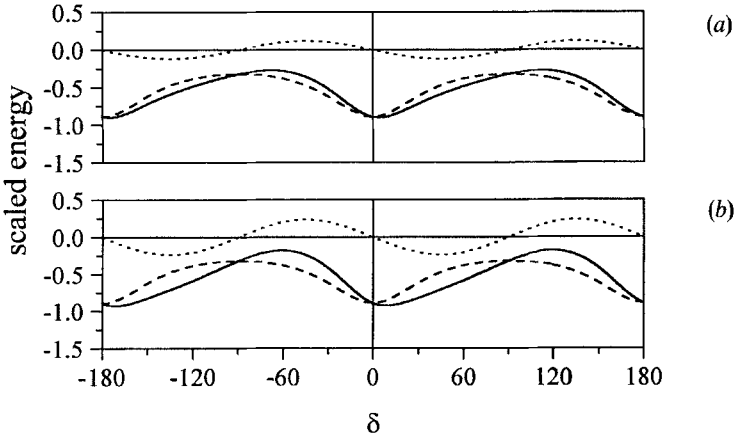

Figure 1. The dependence of the scaled energy on the twist angle δ between the unit vectors $\hat{\mathbf{u}}_1$ and $\hat{\mathbf{u}}_2$ for two molecules separated by $r^* = r/\sigma_0 = 1{\cdot}5$ with $\hat{\mathbf{u}}_1 \perp \mathbf{r}$ and $\hat{\mathbf{u}}_2 \perp \mathbf{r}$. $U^* = aU_a^* + cU_c^*$ (solid lines), aU_a^* (dashed lines), cU_c^* (dotted lines). The potential parameters were given the values used in the MC simulations performed with a constant value of $a = 1$. (*a*) $c = 1{\cdot}0$; (*b*) $c = 2{\cdot}0$.

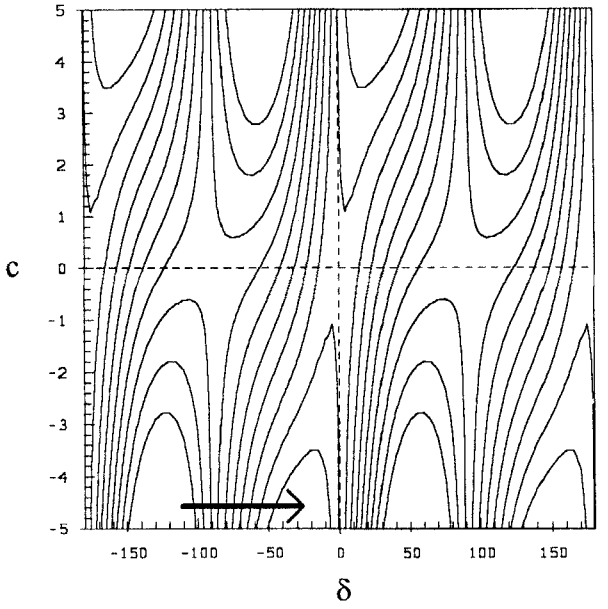

Figure 2. Energy contours for the interaction between two molecules with dependence on the chirality parameter c and twist angle δ for situations as described in figure 1. Following the arrow from left to right, the contours refer to values of U^* decreasing from $-0{\cdot}1$ to $-1{\cdot}0$ in steps of 0·1. The intersections at $c=1{\cdot}0$ and $c=2{\cdot}0$ are shown in figures 1 (*a*) and (*b*), respectively.

3. Computational details

We studied the influence of chirality by investigating a system of $N=256$ molecules in a cubic simulation box using normal Metropolis Monte Carlo technique in the NVT ensemble [23, 24]. Cubic periodic boundary conditions, nearest image summation and a spherical cut-off have been used. In the following, scaled units will be used: scaled temperature $T^*=k_BT/\varepsilon_0$, scaled density $\rho^*=N\sigma_0^3/V$, scaled energy $U^*=U/\varepsilon_0$ and scaled distance $r^*=r/\sigma_0$. The parameter values ($\sigma_e/\sigma_s=3$, $\varepsilon_e/\varepsilon_s=1/5$, $\mu=1$, $\nu=2$) and the simulation conditions ($\rho^*=0{\cdot}30$, cut-off at $r^*=0{\cdot}38$) have been taken from the MD simulation of Luckhurst *et al.* [12]. At each cycle, for each molecule, random translations and rotations were performed in combination. The rotation was applied as proposed by Barker and Watts [25]; the sizes of the rotational and translational moves were adjusted to give an acceptance rate of 50 per cent. All required random numbers have been created using the NAG library routine G05CAF [26].

4. Calculation of order parameters

During the production runs the two second rank order parameters, $\langle P_2\rangle$ and $\langle C\rangle$, characterizing a biaxial phase composed of rotationally symmetric molecules have been calculated similarly to [27]. They are given in terms of orientational distribution coefficients

$$g_{ijkl}=\frac{1}{8\pi^2}\int f(\Omega)a_{ik}(\Omega)a_{jl}(\Omega)\,d\Omega, \tag{10}$$

defined analogously to [28], where Ω comprises the eulerian angles α, β, γ between the space-fixed x_i' and the molecule-fixed x_i coordinate system; a_{ij} are the elements of the

orthogonal transformation matrix from the x_i' to the x_i and $\bar{f}(\Omega)$ describes the orientational distribution function averaged over the simulation box with respect to its positional dependence. The orientational distribution coefficients of equation (10) are thus the mean values over the box of the local coefficients (see Appendix).

For the calculation, the molecule-fixed x_3 axis is chosen parallel to $\hat{\mathbf{u}}_i$ and the symmetric orientational distribution tensor g_{33kl} is computed after each cycle for the present configuration according to the discrete formulation of equation (10),

$$g_{33kl}=\frac{1}{N}\sum_{i=1}^{N} a_{3k}^{(i)} a_{3l}^{(i)}, \tag{11}$$

by averaging over all N molecules in the simulation box.

In order to identify the director in the laboratory frame, g_{33kl} is diagonalized and the eigenvalues g_{33ii}^* $(i=1, 2, 3)$ are arranged in a way to satisfy the relations

$$\left.\begin{aligned} &|g_{3311}^*-g_{3322}^*|<|g_{3311}^*-g_{3333}^*|, \\ \text{and}\quad &|g_{3311}^*-g_{3322}^*|<|g_{3322}^*-g_{3333}^*|, \end{aligned}\right\} \tag{12}$$

where the index* indicates the reference to the principal axes of g_{33kl}. It should be mentioned that the index* as introduced in [29], as well as used in this context, denotes the reference to appropriately chosen molecule-fixed x_i and space-fixed x_i' coordinate systems where all tensors g_{iikl} $(i=1, 2, 3)$ and g_{ijkk} $(k=1, 2, 3)$ are diagonal. In the case of uniaxial phases, as discussed in [29, 30], this is obtained by the choice of the space-fixed x_3' axis parallel to the optical axis, which as a consequence gives diagonal tensors $g_{iikl}(i=1, 2, 3)$ followed by the simultaneous diagonalization of g_{ij33}, g_{ij22}, and g_{ij11}; analogously here, the choice of the molecule-fixed x_3 axis, parallel to the symmetry axis of the rotationally symmetric molecule leading to diagonal tensors g_{ijkk} $(k=1, 2, 3)$ and the subsequent simultaneous diagonalisation of g_{33kl}, g_{22kl}, and g_{11kl}, gives this extraordinary result. The director $\hat{\mathbf{n}}$ is defined here by the eigenvector corresponding to the eigenvalue g_{3333}^*. The order parameters defined by

$$\langle P_2\rangle=\tfrac{1}{2}(3g_{3333}^*-1)=\langle\tfrac{1}{2}(3\cos^2\beta-1)\rangle, \tag{13}$$

and

$$\langle C\rangle=\frac{\sqrt{3}}{2}(g_{3322}^*-g_{3311}^*)=\left\langle -\frac{\sqrt{3}}{2}\sin^2\beta\cos 2\alpha\right\rangle, \tag{14}$$

can now be calculated.

The additional requirement $g_{3322}^*\geqslant g_{3311}^*\geqslant 0$ causes a definite hierarchy of all eigenvalues and restricts the order parameter $\langle C\rangle$ to positive values. It should be mentioned that in the case of biaxial phases with differences $g_{3333}^*-g_{3322}^*$ and $g_{3322}^*-g_{3311}^*$ (related to $g_{3333}^*\geqslant g_{3322}^*\geqslant g_{3311}^*$) of comparable magnitude, a director fluctuation can be caused during a simulation by this algorithm which then should be altered. Then a consideration of all three eigenvalues may be useful in this case.

For a homogeneous orientational distribution in the box, i.e. for nematic phases, the order parameter $\langle P_2\rangle$ is equal to the Saupe order parameter. For inhomogeneous phases as, for example, the cholesteric phase, $\langle P_2\rangle$ has a different meaning. If only segments of a multiple of $p/2$ are considered, p being the pitch, then $\langle P_2\rangle$ describes the local order with respect to the helical axis (see Appendix). Using the arrangement described above $\langle P_2\rangle$ should as usual be zero in an isotropic phase, apart from finite

size corrections. For a homogeneous phase, $\langle P_2 \rangle$ increases to its maximum value of $\langle P_2 \rangle = 1$ if the molecules are arranged with their axis $\hat{\mathbf{u}}_i$ more and more parallel to the director, and decreases to its minimum value of $\langle P_2 \rangle = -0{\cdot}5$ if the molecules are arranged with their axis $\hat{\mathbf{u}}_i$ more and more perpendicular to the director. For each value of $\langle P_2 \rangle$, the biaxiality parameter $\langle C \rangle$ can generally vary between bounds according to the order triangle [30], defined here with $\langle P_2 \rangle$ and $\langle C \rangle$ as orthogonal cartesian coordinates, which is suitable to describe such biaxial phases.

5. Simulation of achiral systems

In order to check our MC program and to obtain suitable well-equilibrated starting configurations for the simulation of chiral systems, we performed a simulation run under conditions comparable to the MD simulations [12]. Starting with an isotropic system at a scaled temperature $T^* = 3{\cdot}0$, we cooled the system down by steps $\Delta T^* = 0{\cdot}25$ to $T^* = 0{\cdot}25$, while each subsequent run was started from the preceding final configuration. At each temperature, an equilibration run about 40 kc (1 kc denotes 1000 attempted moves per particle) was followed by a production run about 80 kc. Additionally, the simulation runs were operated on heating up the system. In figure 3 we show the calculated order parameter values together with the values obtained by Luckhurst *et al.*, using MD [12], as a function of the scaled temperature. The good agreement of the MC and MD results and the well-known behaviour of the Gay–Berne fluid is obvious: on cooling, spontaneously ordered states appear, characterized as nematic and smectic phases by correlation functions and visualizations of selected configurations given in detail elsewhere [12, 16, 31]. The phase biaxility $\langle C \rangle$ was found to be negligible for all simulated systems.

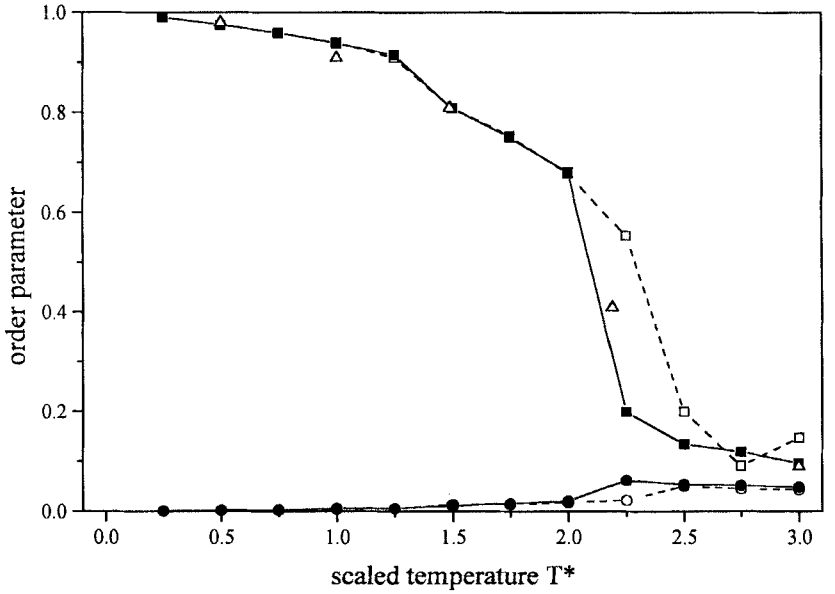

Figure 3. The order parameters $\langle P_2 \rangle$ (squares) and $\langle C \rangle$ (circles) for the achiral system ($c = 0$) as functions of the scaled temperature T^*. Filled symbols joined by solid lines denote results of runs progressing from high to low temperature; open symbols joined by dashed lines are results of runs from low to high temperature. Additionally, MD results for $\langle P_2 \rangle$ (triangles) are given as taken from [12]. All order parameters have been calculated using $g^*_{3333} \geqslant g^*_{3322} \geqslant g^*_{3311}$.

6. Simulation of chiral systems

In order to investigate the influence of chirality, the phase diagram of the chiral Gay–Berne fluid in the chirality–temperature plane was analysed along two selected intersections: sequences of runs along the isotherm $T^* = 1{\cdot}50$, by variation of the chirality parameter c, and along the isochiral $c = 0{\cdot}80$, by variation of temperature, were performed. Each run was started from the final configuration of a simulation at a nearby value for the chirality parameter or temperature respectively. In order to check against metastability, the whole simulation sequences were repeated in the opposite direction. Usually, at each point, an equilibration run of 100 kc was followed by a production run of the same length.

6.1. *Variation of chirality along an isotherm*

Starting from the obtained nematic phase at $T^* = 1{\cdot}50$ with $c = 0$, the chirality parameter was increased along this isotherm by steps $\Delta c = 0{\cdot}1$ up to $c = 2{\cdot}0$. The values obtained for the average chiral energy contributions are given in figure 4 as functions of the chirality parameter c. Significant changes allowing an approximate localization of resulting phase transitions appear. A first phase transition is obvious in the region $0{\cdot}6 \leqslant c \leqslant 0{\cdot}7$; on increasing the chirality parameter, a second phase transition takes place in the region $1{\cdot}0 \leqslant c \leqslant 1{\cdot}1$. It is quite possible that much longer runs will reveal the metastable character of some state points close to the transition which then will occur at even lower values of c as indicated by the results of the runs with decreasing chirality. Additionally further phase transitions are indicated at high values of the chirality parameter which are still under investigation and therefore not discussed in the following. First information about the nature of the phases is given by the values obtained for the order parameters $\langle P_2 \rangle$ and $\langle C \rangle$ shown in figure 5 as functions of the chirality parameter.

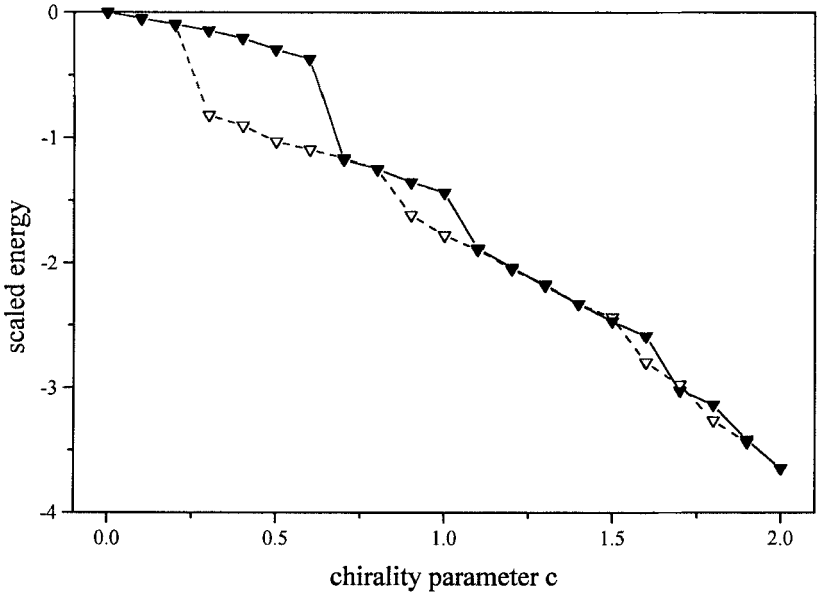

Figure 4. The chiral energy contribution $\langle U_c^* \rangle$ (triangles) as a function of the chirality parameter c along the isotherm $T^* = 1{\cdot}50$. Filled symbols joined by a solid line denote results of runs progressing from low to high chirality parameter; open symbols joined by a dashed line denote results of runs from high to low chirality parameter.

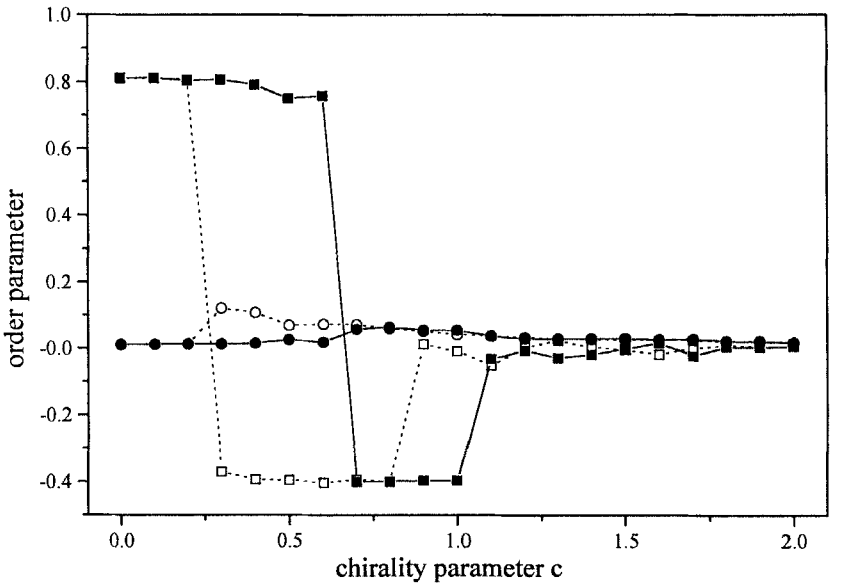

Figure 5. The order parameters $\langle P_2 \rangle$ (squares) and $\langle C \rangle$ (circles) as functions of the chirality parameter c along the isotherm $T^* = 1{\cdot}50$. Filled symbols joined by solid lines denote results of runs progressing from low to high chirality parameter; open symbols joined by dashed lines denote results of runs from high to low chirality parameter.

For low values of c, the order parameter $\langle P_2 \rangle \approx 0{\cdot}8$ indicates a favoured parallel orientation of the unit vectors $\hat{\mathbf{u}}_i$ with respect to the director, i.e. the usual behaviour of nematics. The phase biaxiality of the system is negligible as shown by the very small values of $\langle C \rangle$ in comparison to $\langle P_2 \rangle$. At the first phase transition, the favoured orientation has dramatically changed: now for an intermediate chirality parameter, an orientation of the unit vectors $\hat{\mathbf{u}}_i$ perpendicular to the director is preferred as indicated by values $\langle P_2 \rangle \approx -0{\cdot}4$ close to the minimum value $\langle P_2 \rangle = -0{\cdot}5$. The apparent phase biaxiality is again weak, but increased. For high values of c again strong changes appear. The value of $\langle P_2 \rangle$ is fluctuating around zero, indicating the isotropic character of the phase. A visualization of the arrangement of the molecules using the final configuration of selected production runs allows, in a simple way, a further characterization to be made. In figure 6 we show images of the two phases obtained by runs with increasing chirality parameter: the snapshot related to $c = 0{\cdot}9$ shows the characteristics of a cholesteric phase; on the contrary at $c = 1{\cdot}3$ features of a blue phase can be seen.

Characteristic for the cholesteric phase (figure 6, left) is the periodic change of the favoured molecule orientation along the helical axis given here by x'_3, as illustrated in figure 6 (*b*) and (*c*) and the isotropic distribution of the molecular centres in the x'_1, x'_2-plane, whereas always an orientation perpendicular to the helical axis is preferred, as is obvious in figure 6 (*a*).

The similarity of the blue phase obtained (figure 6, right) to the model of BPII [19, 33, 34], given for comparison in figure 7, is evident: the images show the characteristics of double twist cylinders in a cubic arrangement.

In order to elucidate the structural features of the phases appearing, a longitudinal orientational pair correlation function of rank two defined by

$$g_2(r_\parallel^*) = \langle P_2(\cos \delta_{ij}(r_\parallel^*)) \rangle, \tag{15}$$

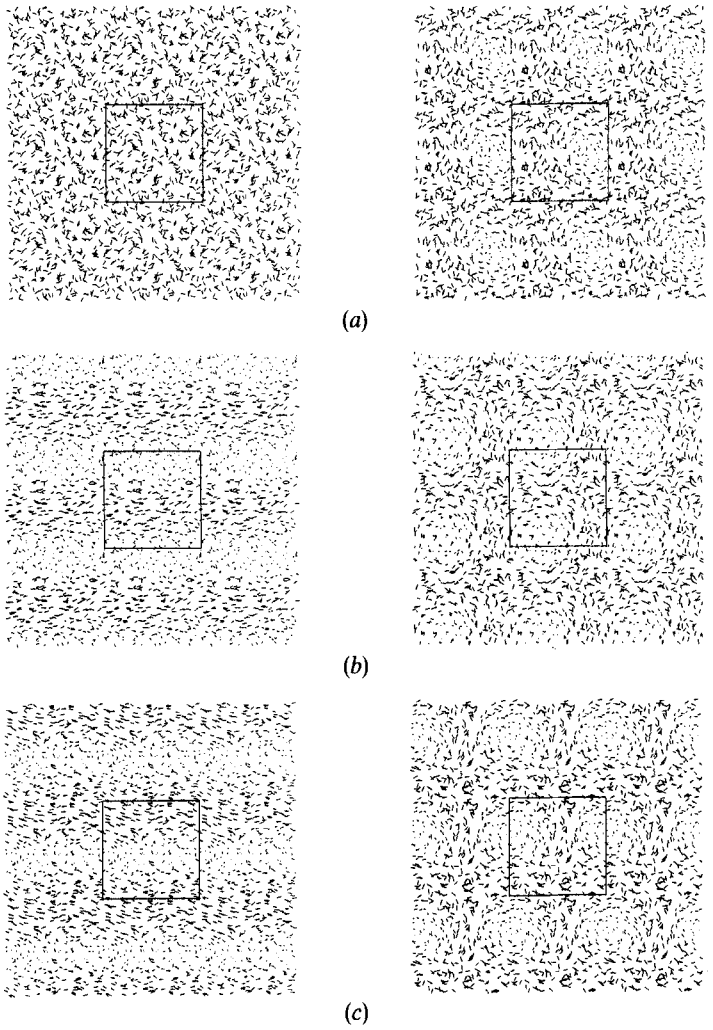

Figure 6. Final configurations of the production runs at $c=0{\cdot}9$ (left) and $c=1{\cdot}3$ (right). Each molecule is represented as a line in the shown projections of the system into the (*a*) x'_1, x'_2 plane, (*b*) x'_1, x'_3 plane, and (*c*) x'_2, x'_3 plane created with the molecular modelling program QUANTA [32]. In order to yield a better impression of the arrangement, the central simulation box (□) is surrounded by its identical images as given by the use of periodic boundary conditions.

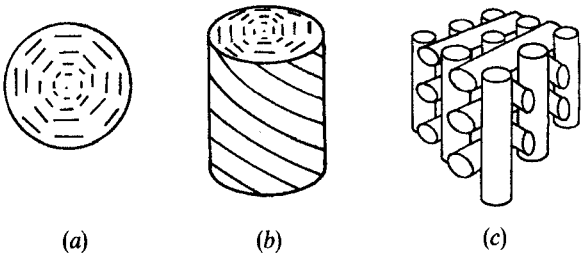

Figure 7. Theoretical model of BPII: (*a*) top view of a double twist cylinder; (*b*) side view of a double twist cylinder; (*c*) three dimensional arrangement (figures from [34]).

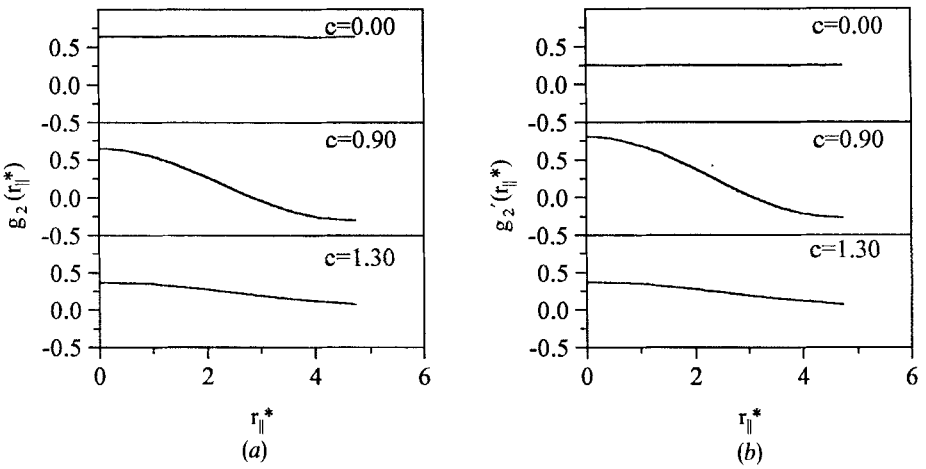

Figure 8. Longitudinal orientational pair correlation functions (*a*) $g_2(r_\parallel^*)$ and (*b*) $g_2'(r_\parallel^*)$ and their dependence on the chirality parameter: $c=0{\cdot}0$ (nematic); $c=0{\cdot}9$) cholesteric); $c=1{\cdot}30$ (blue phase). In the case of the blue phase, $r_\parallel^*$ was taken as the distance in the direction of the normal vector of one arbitrarily chosen box face.

was calculated, where P_2 is the second order Legendre polynomial and $\delta_{ij}(r_\parallel^*)$ denotes the angle between $\hat{\mathbf{u}}_i$ and $\hat{\mathbf{u}}_j$ of two selected molecules separated by a scaled distance $r_\parallel^*$ in the direction parallel to the director. This correlation function depends on both Eulerian angles α and β; therefore the similar function

$$g_2'(r_\parallel^*)=\langle P_2(\cos\delta_{ij}'(r_\parallel^*))\rangle \tag{16}$$

independent of β and thus of the degree of order given by $\langle P_2\rangle$ was evaluated where now δ_{ij}' is the angle between the projections of $\hat{\mathbf{u}}_i$ and $\hat{\mathbf{u}}_j$ into the plane perpendicular to the director.

For all three analysed phases the functions given in figure 8 show significant differences; especially evident is the behaviour for the cholesteric phase. Whereas for the nematic phase $g_2(r_\parallel^*)$ and $g_\parallel'(r_\parallel^*)$ are constant over the whole range, for the cholesteric phase they vary with $r_\parallel^*$. They change monotonously from their maximum values close to 1·0, indicating a preferred orientation with a small twist angle for molecules separated by small values of $r_\parallel^*$ to their minimum values close to $-0{\cdot}5$ for molecules separated by half of the box length in the direction parallel to the director, indicating a preferred orientation of these molecules perpendicular to each other. The functions show additionally that only a part of a helix with the length of the half pitch has been formed inside the simulation cell. In the case of the blue phases, the functions obtained for the three different normal vectors of the box show the same behaviour as given here and are therefore not shown separately, documenting the equivalence of three distinguished orthogonal directions in the case of BPII.

6.2. *Variation of temperature along an isochiral*

Using the isotropic phase obtained at $T^*=3{\cdot}0$ with $c=0$ as the initial configuration, the temperature is now reduced by steps $\Delta T^*=0{\cdot}25$ down to $T^*=0{\cdot}25$ along the isochiral with $c=0{\cdot}8$. With decreasing temperature, the orientation perpendicular to the director is favoured more and more as indicated by the order parameter $\langle P_2\rangle$ given in figure 9. Again helical phases appear, as illustrated in figure 10 (*a*) by the behaviour of the longitudinal orientational pair correlation functions $g_2(r_\parallel^*)$ and $g_2'(r_\parallel^*)$. But now,

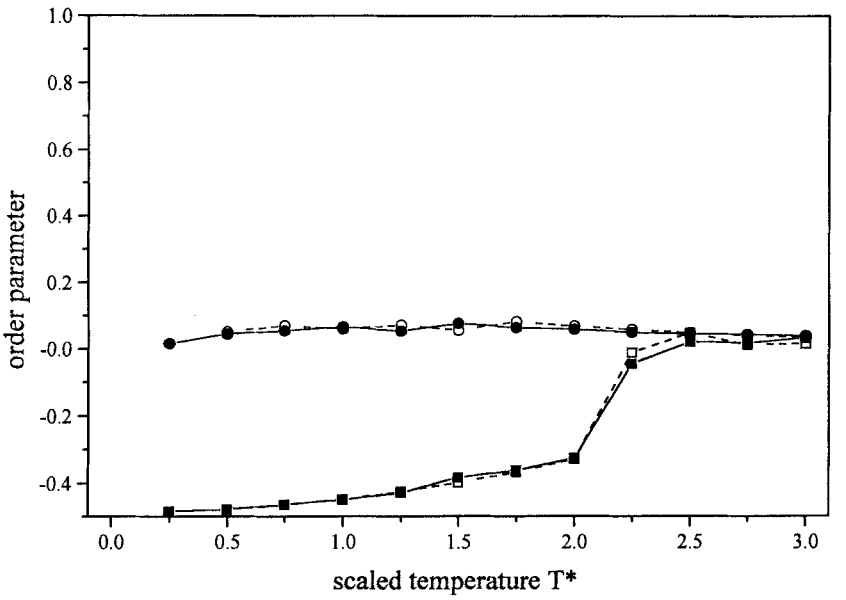

Figure 9. The order parameters $\langle P_2 \rangle$ (squares) and $\langle C \rangle$ (circles) as functions of the scaled temperature T^* along the isochiral $c = 0{\cdot}8$. Filled symbols joined by solid lines denote results of runs progressing from high to low temperature, open symbols joined by dashed lines denote results of runs from low to high temperature.

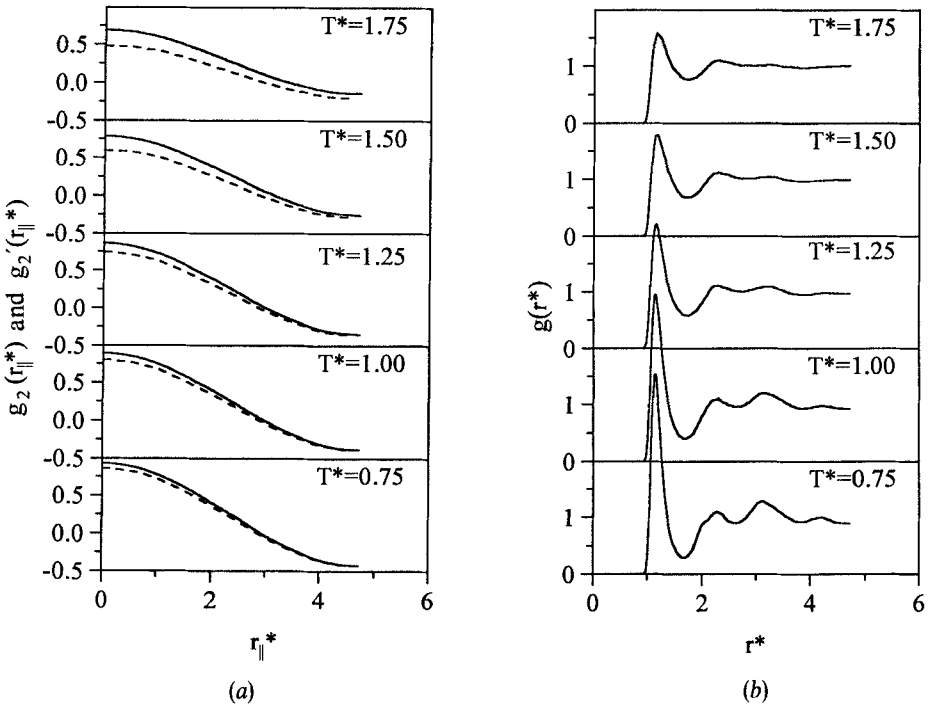

Figure 10. Correlation functions and their dependence on the scaled temperature T^* at $c = 0{\cdot}8$: (*a*) longitudinal orientational pair correlation functions: g_2 ($r_\parallel^*$) (solid lines), g_2' ($r_\parallel^*$) (dashed lines); (*b*) radial distribution functions.

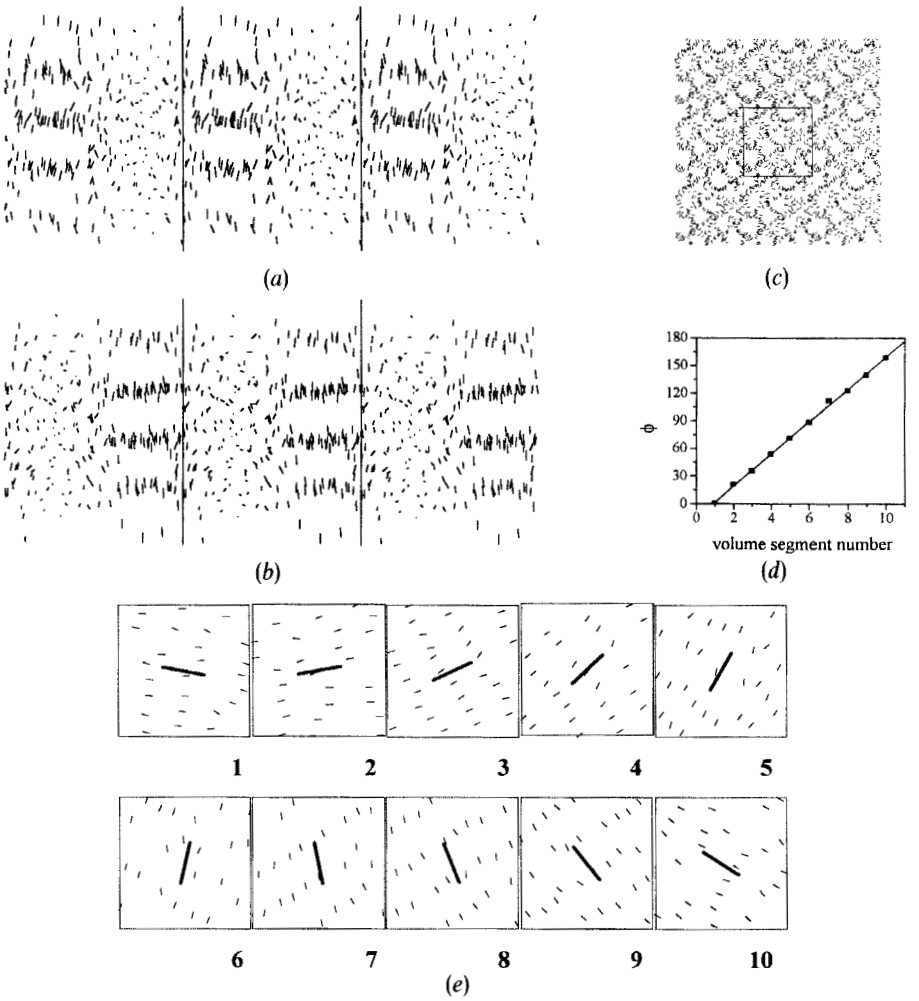

Figure 11. Final configuration of the production run at $c=0{\cdot}8$ and $T^*=0{\cdot}75$. The images (*a*) and (*b*) show the same snapshot only rotated by 90° against each other around the horizontally oriented helical axis. The central simulation box is surrounded by its identical images in the direction of the helical axis. Additionally, projections of the simulation box (□) surrounded by its identical images (*c*) and of volume segments chosen perpendicular to the helical axis (*e*) into the x'_1, x'_2 plane are given. For each volume segment a local director has been calculated according to §4, of which the normalized projection into the x'_1, x'_2 plane is shown by a heavy line. In (*d*), the angle of rotation ϕ of the projections of the so-defined local directors is given as a function of the volume segment number.

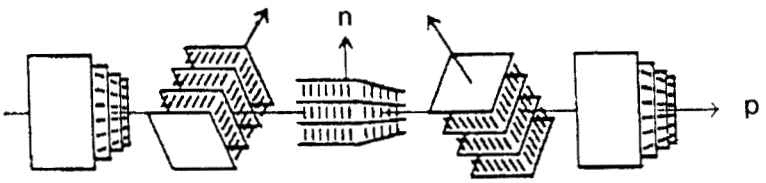

Figure 12. Model for the helical smectic A* phase (figure from [36]).

additionally increasing positional correlations are obvious as shown in figure 10 (*b*) by the radial distribution function $g(r^*)$. In figure 11, a configuration obtained with $c = 0{\cdot}8$ and $T^* = 0{\cdot}75$ is shown which demonstrates the appearance of a spiraling layer order, typical for the model of the helical smectic A* phase, given, for comparison, in figure 12, as predicted by Renn and Lubensky [35] and discovered by Goodby *et al.* [20].

7. Discussion

In the preceding sections, we have described the results of our Monte Carlo studies for a system of chiral particles with interactions described by the Gay–Berne potential and an additive chiral potential, a system for convenience denoted as chiral Gay–Berne fluid. This system shows different chiral phases, as temperature and chirality parameter are varied, which have been characterized as cholesteric, helical smectic and blue phases by the use of correlation functions, order parameters and visualizations of selected configurations using computer graphics. These phases have to be discussed here especially under the restrictions given by the applied periodic boundary conditions and the small system size, respectively.

In the case of the cholesteric phase, we have found that, independent of temperature and chirality parameter values, a part of a helix with a length of a half pitch was always formed inside the simulation box, while the helical axis was parallel to one of the normal vectors of the cubic box. Both facts can be easily understood considering the boundary conditions: in order to harmonize with its own periodic images, a repeatable part of the helix must fit exactly into the simulation box. This requirement is fulfilled by all parts of a helix with length $n(p/2)$ where p denotes the pitch and n stands for a positive integer. Due to the small system size, only helices with $n = 1$ have been formed in such a way as to obtain the maximum pitch $p = 2L$, i.e. avoiding oblique orientations of the helical axis in the cubic simulation box of length L. These boundary effects simultaneously explain the threshold value obtained for the chirality parameter necessary for the formation of a cholesteric phase, as found by simulations along an isotherm with increasing chirality parameter. For values of the chirality parameter below the threshold value, a cholesteric phase would be favoured with a pitch greater than twice the box length, a situation prevented by the boundary conditions used. The cholesteric phases obtained, therefore, represent in general no undisturbed helical structures. It can be expected that by analogy with the case of the Cano wedge, where as a function of the distance between the two surfaces undisturbed helical structures have compressed or stretched helical structures as neighbours, these situations depend here on the given box size, fixed by the number of molecules under investigation.

Simulations of larger systems, therefore, should yield a systematic lowering of the threshold value. Simultaneously, the variation of the molecule number at constant values of density, temperature and chirality parameter should allow the detection of the undisturbed helical structure, i.e., the pitch due to the selected parameters, by searching for the minimum of energy. The use of a rectangular simulation cell instead of a cubic box should help to reduce the enormous amount of computational time necessary for such investigations. In order to overcome these problems and to analyse especially the temperature dependence of the helical pitch NpT, simulations allowing a change of box size and hence the formation of undisturbed helical structures would be preferable to NVT simulations. A very interesting possibility could be the use of a special twisted simulation cell, as pointed out by Yoneya and Berendsen [37], which would allow helical structures with a pitch much longer than that fixed by the box size.

In principle, these considerations are also valid for the helical smectic phase. For a detailed analysis of its structure and especially of the order in the smectic layers, larger system sizes are required. The restrictions due to the periodic boundary conditions can be seen even more strongly in the case of the blue phase. Here the axes of all double twist cylinders are constrained to the normals of the cubic simulation cell, allowing in this way the formation of a suitable unit cell which fits well inside the simulation box. The region of existence of the blue phase (until now proved only by the visual impression of selected configurations in common with values of the order of parameter $\langle P_2 \rangle$ close to zero calculated with the algorithm described in §4 and not by suitable correlation functions) should possibly move to higher values of the chirality parameter if larger systems are investigated. According to many experimental results [38], the formation of blue phases is favoured in systems with a very small pitch, conditions which are given here in advance by the chosen boundary conditions.

Considering that only two parameters of the model—temperature and chirality parameter—have been changed in this study, the rich polymorphism of the chiral Gay–Berne model is remarkable and should give reasons for further investigation in spite of the above mentioned restrictions, allowing a more detailed characterization of the different phases. Promising aspects consist in a modification of the chiral potential used here in order to investigate the phenomenon of induced cholesteric phases by a simulation of guest–host systems, in combination with the use of suitable boundary conditions.

Financial support by the Fonds der Chemischen Industrie and generous allocation of computer time by the Regionales Hochschulrechenzentrum Kaiserslautern are gratefully acknowledged.

Appendix

In order to illustrate the meaning of the order parameters calculated according to §4 and the longitudinal orientational pair correlation function, special situations will be treated here. All statements are related to systems consisting of rotationally symmetric molecules with the molecule-fixed x_3 axis chosen to be parallel to the symmetry axis of the molecule.

(*a*) Uniaxial nematic phase, where all molecules are oriented parallel to each other: $\langle P_2 \rangle = 1$, $\langle C \rangle = 0$, with $\hat{\mathbf{n}}$ parallel to the optical axis.

(*b*) Uniaxial nematic phase, where all molecules are oriented perpendicular to the optical axis: $\langle P_2 \rangle = -\frac{1}{2}$, $\langle C \rangle = 0$, with $\hat{\mathbf{n}}$ parallel to the optical axis.

(*c*) Cholesteric phase: The values of $\langle P_2 \rangle$, $\langle C \rangle$, and the orientation of $\hat{\mathbf{n}}$ depend on the segment of the helix taken into account by the calculation. However, segments of a multiple of $p/2$ can be treated as a special case. Starting from the local orientation distribution function $f(z, \Omega)$ with z in the direction of the helical axis, one obtains local orientational distribution coefficients $g_{ijkl}(z)$. Averaging these coefficients over segments of a multiple of $p/2$ yields

$$g_{33kl} = \begin{bmatrix} \frac{1}{2}[1 - g_{3333}(z_0)] & 0 & 0 \\ 0 & \frac{1}{2}[1 - g_{3333}(z_0)] & 0 \\ 0 & 0 & g_{3333}(z_0) \end{bmatrix},$$

i.e. $g_{3333} = g_{3333}(z_0)$. Therefore, $\langle C \rangle = 0$, and in the case of a locally uniaxial system, the order parameter $\langle P_2 \rangle$ describes the local order with respect to the helical axis which is parallel to $\hat{\mathbf{n}}$. If all molecules are oriented perpendicular to $\hat{\mathbf{n}}$, one gets again $\langle P_2 \rangle = -\frac{1}{2}$.

In order to distinguish between (*b*) and (*c*) is it suitable to look at the longitudinal orientational pair correlation function $g'_2(r^*_\parallel)$. Whereas in (*b*) $g'_2(r^*_\parallel) = \frac{1}{4}$ is independent of $r^*_\parallel$, in (*c*) this function varies according to $g'_2(r^*_\parallel) = \frac{1}{2}(3\cos^2[(2\pi/p)r^*_\parallel] - 1)$ if, in each layer perpendicular to the helical axis, all molecules are oriented parallel to each other.

References

[1] ALLEN, M. P., and WILSON, M. R., 1989, *J. Comput.-Aided Molec. Design*, **3**, 335.
[2] LEBWOHL, P. A., and LASHER, G., 1972, *Phys. Rev.* A, **6**, 426.
[3] FRENKEL, D., 1987, *J. phys. Chem.*, **91**, 4912.
[4] STROOBANTS, A., LEKKERKERKER, H. N. W., and FRENKEL, D., 1987, *Phys. Rev.* A, **36**, 2929.
[5] FRENKEL, D., 1989, *Liq. Crystals*, **5**, 929.
[6] ONSAGER, L., 1949, *Ann. N.Y. Acad. Sci.*, **51**, 627.
[7] WILSON, M. R., and ALLEN, M. P., 1991, *Molec. Crystals liq. Crystals*, **198**, 465.
[8] WILSON, M. R., and ALLEN, M. P., 1992, *Liq. Crystals*, **12**, 157.
[9] GAY, J. G., and BERNE, B. J., 1981, *J. chem. Phys.*, **74**, 3316.
[10] BERNE, B. J., and PECHUKAS, P., 1972, *J. chem. Phys.*, **56**, 4213.
[11] ADAMS, D. J., LUCKHURST, G. R., and PHIPPEN, R. W., 1987, *Molec. Phys.*, **61**, 1575.
[12] LUCKHURST, G. R., STEPHENS, R. A., and PHIPPEN, R. W., 1990, *Liq. Crystals*, **8**, 451.
[13] EMSLEY, J. W., LUCKHURST, G. R., PALKE, W. E., and TILDESLEY, D. J., 1992, *Liq. Crystals*. **11**, 519.
[14] EMERSON, A. P. J., HASHIM, R., and LUCKHURST, G. R., 1992, *Molec. Phys.*, **76**, 241.
[15] DE MIGUEL, E., RULL, L. F., CHALAM, M. K., GUBBINS, K. E., and VAN SWOL, F., 1991, *Molec. Phys.*, **72**, 593.
[16] DE MIGUEL, E., RULL, L. F., CHALAM, M. K., and GUBBINS, K. E., 1991, *Molec. Phys.*, **74**, 405.
[17] TSYKALO, A. L., 1991, *Thermophysical Properties of Liquid Crystals* (Gordon & Breach), Chap. 7.
[18] GOODBY, J. W., 1991, *J. mater. Chem.*, **1**, 307.
[19] WRIGHT, D. C., and MERMIN, N. D., 1989, *Rev. mod. Phys.*, **61**, 385.
[20] GOODBY, J. W., WAUGH, M. A., STEIN, S. M., CHIN, E., PINDAK, R., and PATEL, J. S., 1989, *J. Am. chem. Soc.*, **111**, 8119.
[21] VAN DER MEER, B. W., VERTOGEN, G., DEKKER, A. J., and YPMA, J. G. J., 1976, *J. chem. Phys.*, **65**, 3935.
[22] OSIPOV, M. A., 1993, *Liquid Crystalline and Mesomorphic Polymers*, edited by V. P. Shibaev and L. Lam (Springer) (in the press).
[23] METROPOLIS, N., ROSENBLUTH, A. W., ROSENBLUTH, M. N., TELLER, A. H., and TELLER, E., 1953, *J. chem. Phys.*, **21**, 1087.
[24] ALLEN, M. P., and TILDESLEY, D. J., 1987, *Computer Simulation of Liquids* (Oxford University Press).
[25] BARKER, J. A., and WATTS, R. O., 1969, *Chem. Phys. Lett.*, **3**, 144.
[26] NAG, 1984, NAG Fortran Library Manual.
[27] ZANNONI, C., 1979, *The Molecular Physics of Liquid Crystals*, edited by G. R. Luckhurst and G. W. Gray (Academic Press), Chap. 3.
[28] KUBALL, H.-G., ALTSCHUH, J., and SCHÖNHOFER, A., 1980, *Chem. Phys.*, **49**, 247.
[29] SCHWABEN, H. D., WEILAND, R., DOLLE, V., STRAUSS, A., and KUBALL, H.-G., 1984, *Abstracts of 14. Freiburger Arbeitstagung Flüssigkristalle*, Freiburg, Germany.
[30] KUBALL, H.-G., STRAUSS, A., KAPPEL, M., FECHTER-RINK, E., SCHÖNHOFER, A., and SCHEROWSKY, G., 1987, *Ber. Bunsenges. phys. Chem.*, **91**, 1266.
[31] MEMMER, R., 1992, Dissertation, Universität Kaiserslautern.
[32] QUANTA (Version 3.2, Polygen, Waltham, Massuchusetts 02254, U.S.A.).

[33] CROOKER, P. P., and KITZEROW, H.-S., 1992, *Cond. Mat. New.*, **1,** 6.
[34] COLLINGS, P. J., 1990, *Liquid Crystals–Nature's Delicate Phase of Matter* (Hilger).
[35] RENN, S. R., and LUBENSKY, T. C., 1988, *Phys. Rev.* A, **38,** 2132.
[36] RENN, S. R., and LUBENSKY, T. C., 1991, *Molec. Crystals liq. Crystals*, **209,** 349.
[37] YONEYA, M., and BERENDSEN, H. J. C., 1992, *Abstracts of 14 International Liquid Crystal Conference*, Pisa, Italy.
[38] ONUSSEIT, H., and STEGEMEYER, H., 1982, *Chem. Phys. Lett.*, **89,** 95.